The College of Engineering
University of Wisconsin-Madison

Wisconsin Electric Machines and Power Electronics Consortium

RESEARCH REPORT
86-9

Operation of Naturally Sampled Current Regulators in the Transition Mode

T. M. Rowan and R. J. Kerkman
Allen-Bradley Company
1201 South Second Street
Milwaukee, WI 53204

T. A. Lipo
University of Wisconsin
1415 Johnson Drive
Madison, WI 53706

WEMPEC

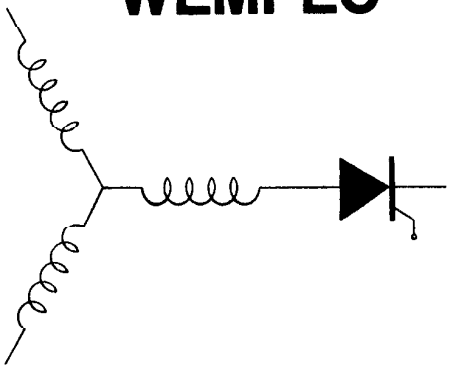

Department of Electrical and Computer Engineering
1415 Johnson Drive
Madison, Wisconsin 53706

June 1986

Operation of Naturally Sampled Current Regulators in the Transition Mode

TIMOTHY M. ROWAN, MEMBER, IEEE, RUSSEL J. KERKMAN, MEMBER, IEEE, AND THOMAS A. LIPO, FELLOW, IEEE

Abstract—**A fundamental component model of current-regulated naturally sampled PWM inverters operating in the pulse-dropping mode is proposed. Analytical and test results are compared for purposes of model verification and regulator evaluation. The results demonstrate the problems with the classical (stationary reference frame) current regulator that occur in this region of operation. In contrast, the synchronous reference frame regulator is shown to have ideal steady-state response in this region.**

I. Introduction

A FIELD-ORIENTED control strategy is often employed in high-performance ac drives. This strategy decouples the ac machine so that independent torque and flux control are provided, as in a dc machine. An integral element in such a scheme is a method to control the stator currents. This often is accomplished through the use of high-gain PWM current inverters, often referred to as current-regulated PWM (CRPWM) inverters.

There are two main types of CRPWM inverters, the hysteretic and the sine-triangle comparison regulator. The sine-triangle comparison regulator employs a naturally sampled PWM algorithm with proportional–integral (PI) compensation in the feedforward path of the current feedback loops. This regulator has gained popularity over the hysteretic regulator because, over a wide range of operating conditions, it has a constant switching frequency and is essentially a linear controller.

An observable characteristic of the naturally sampled linear regulator is its deterioration in steady-state current regulation at higher operating frequencies [1]–[4]. This phenomenon has been analyzed in the literature [5] and shown to be an inherent characteristic of the classical (stationary reference frame) regulator. The paper of [5] proposed and demonstrated that a synchronous reference frame current regulator provides the ideal steady-state current regulation that the classical uncompensated regulator cannot provide. In addition, the paper proposed an equivalent to the synchronous regulator that permits perfect steady-state ac current regulation. This stationary equivalent to the synchronous current regulator provides the ideal current regulation necessary for accurate current control; additional transformations associated with the synchronous regulator are not required, nor is load-dependent compensation, as is the case with the classical regulator.

Neither the classical nor the synchronous naturally sampled current regulators maintain a constant switching frequency over their entire range of operation. After a certain terminal voltage level is reached, any further increase in voltage results in a continual decrease in the PWM switching frequency until the inverter is producing a conventional six-step voltage. This pulse-dropping phenomenon is inherent to the naturally sampled PWM algorithm and results in a nonlinear transition from current control to voltage control. The operation of the classical current regulator in conjunction with a three-phase induction motor in this transition region is characterized by a rapid deterioration in current regulation. This deterioration proceeds as a function of operating frequency, concluding with a discrete jump into the six-step region of operation.

As a consequence of these characteristics, the field-oriented control's torque regulation deteriorates in this region. Moreover, the discrete jump into six-step voltage operation causes an undesirable current transient. Thus the operation of the classical current regulator in the transition region decreases the speed and torque range over which current can be regulated and necessitates a derating of the inverter.

The nonlinearities of the naturally sampled PWM algorithm, which are responsible for transition region operation of the current regulators, also present problems during the open-loop operation of voltage PWM inverters. These problems are not as severe as those of the current regulators, and can be solved by means of sophisticated modulation strategies [6]–[11]. These schemes, though, are not readily adaptable to current-regulated inverters because of their open-loop nature.

In this paper, a fundamental component model of a naturally sampled current-regulated three-phase induction motor operating in the transition region will be developed and experimentally verified. This model will be used to explain the undesirable characteristics of the classical current regulator in this region. The use of a synchronous current regulator [5] will then be proposed to improve the response of current regulators in the transition region. Experimental results from this regulator will be shown and a comparison of the two regulators' operation will be performed using the developed model.

II. Steady-State Operation

The basic configuration of the PWM current regulator that will be studied is shown in Fig. 1. This figure shows that the

Paper IPCSD 86-71, approved by the Industrial Drives Committee of the IEEE Industry Applications Society for presentation at the 1986 Industry Applications Society Annual Meeting, Denver, CO, September 28–October 3. Manuscript released for publication January 22, 1987.

T. M. Rowan and R. J. Kerkman are with the Allen-Bradley Company, 1201 South Second Street, Milwaukee, WI 53204.

T. A. Lipo is with the Department of Electrical and Computer Engineering, University of Wisconsin—Madison, 1415 Johnson Drive, Madison, WI 53706.

IEEE Log Number 8714274.

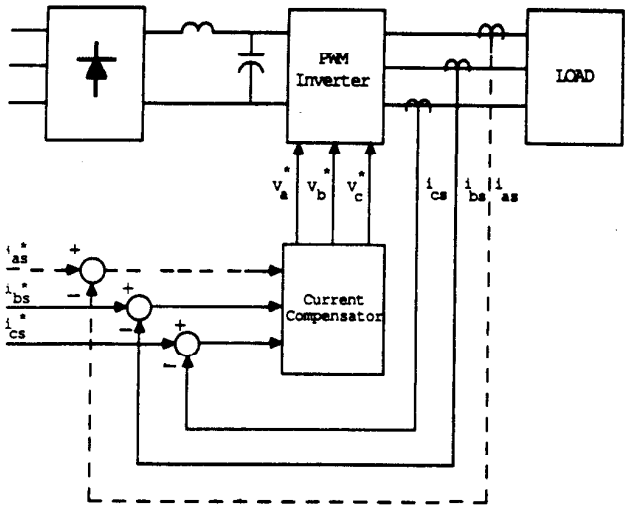

Fig. 1. PWM current regulator configuration.

voltage commands that are presented to the PWM inverter are the result of compensated current error signals. The PWM voltage inverter employs a naturally sampled PWM algorithm. In this section the steady-state operation of the current regulators in the pulse-dropping mode will be examined.

Particular characteristics of the natural sampling PWM algorithm cause the current regulators to exhibit three different modes of steady-state operation. The linear region of operation is characterized by a constant switching frequency. The regulator is in this region of operation whenever the peak of the modulating voltage command is less than the peak of the triangle carrier wave, as illustrated in Fig. 2(a).

The next region of operation, designated as the transition region, is characterized by its pulse-dropping phenomenon. This occurs because the peak of the voltage command is greater than the peak of the triangle wave, as illustrated in Fig. 2(b). Pulse dropping starts to occur when the commanded fundamental component of terminal voltage is 78.5 percent ($\pi/4$) of the fundamental component of the classical six-step wave and increases until each transistor is switching at the operating frequency, resulting in the classic six-step waveform.

The third mode of operation is the six-step mode, caused by the modulating wave totally saturating the triangle wave, as shown in Fig. 2(c).

A. Fundamental Component Model of the PWM Inverter

A fundamental component model of the current-regulated system in the transition region of operation will be developed. This type of model has been long accepted for analysis purposes because the induction machine responds primarily to the fundamental component of the applied voltage.

The naturally sampled PWM inverter has been modeled on a fundamental component basis as a constant gain of $V_{bus}/(2^*A_t)$ in the linear region by many authors [1], [4], [5]. In this gain equation V_{bus} represents the voltage of the dc bus and A_t represents the peak of the triangle wave. This model will not suffice for the transition region, however, due to its

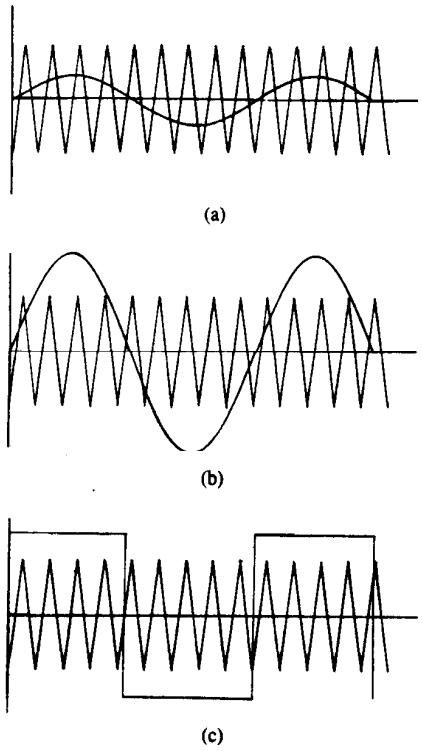

Fig. 2. Voltage command signal and carrier signal for one phase of PWM inverter. (a) Linear region of operation. (b) Transition region of operation. (c) Six-step region of operation.

nonlinearities. When the PWM modulating signal exceeds the peak of the carrier wave, that portion of the signal no longer affects the output voltage, resulting in a voltage that is smaller than commanded. On a fundamental component basis this is manifested as a nonlinear reduction in gain. If it is assumed that the carrier frequency is much greater than the operating frequency, the fundamental component operation in this region is continuous and can be modeled using describing function techniques [12]. The describing function provides a fundamental component representation of a nonlinear element. It assumes a sinusoidal input to a nonlinear element and determines the magnitude and phase shift of the fundamental component of the corresponding output of that element.

To normalize the modulating wave input to the nonlinear block, the concept of modulation index is introduced. The modulation index M_i is defined as the ratio of the peak of the input signal to the triangle wave amplitude. Thus a modulation index greater than unity corresponds to transition region operation. Fig. 3 shows the fundamental component of output voltage versus the modulation index for one phase of a naturally sampled PWM scheme. The output increases linearly until the transition mode is reached, where it increases nonlinearly, asymptotically approaching a value of $2/\pi^*V_{bus}$. This value corresponds to a six-step inverter output. This relationship suggests that the transition mode of the natural sampling algorithm could be modeled as a saturating element with a describing function that has a gain given by (1) with no phase shift [13]. Fig. 4 is a plot of (1); it shows the reduction in gain as a function of input. This plot contains the same

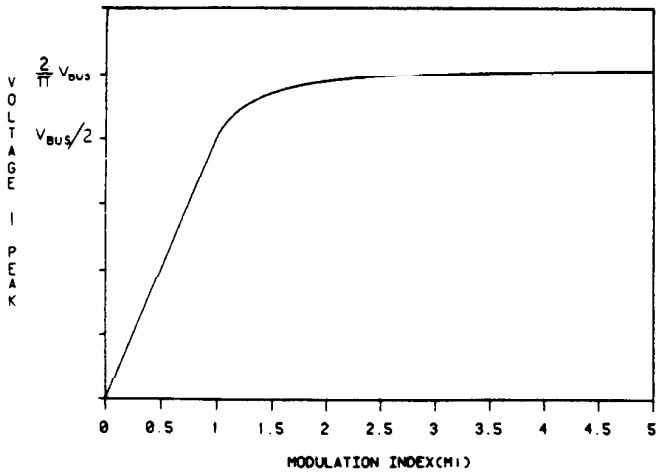

Fig. 3. Fundamental component of phase voltage versus modulation index (M_i).

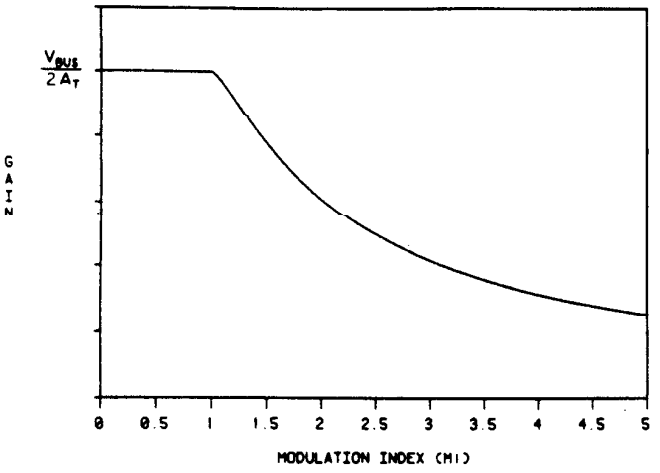

Fig. 4. Fundamental component PWM gain versus modulation index (M_i).

information as Fig. 3, presenting it as a gain relationship rather than as an input–output relationship.

$$G = V_{bus}/(\pi A_t)\ [\sin^{-1}(1/M_i) + (1/M_i)\sqrt{1-(1/M_i)^2}]. \quad (1)$$

Fig. 5 shows the complete system model of the current-regulated systems that will be studied. Since the current regulator is often employed in a field-oriented control application, the inputs and outputs of the model are currents in the synchronous reference frame. The current compensator block consists of PI regulators in both axes. The classical regulator performs the compensation in the stationary reference frame while the synchronous regulator performs the regulation in the synchronous reference frame. The equations representing both types of compensators are presented in detail in [5]. The load is a three-phase induction motor. The gain associated with the PWM inverter is represented in this model as the gain block G, which for the linear region of operation is a constant. Thus, to obtain the steady-state operating point in the linear region, the solution of a set of linear equations is simply required. Conversely, the steady-state solution of the transition region cannot be found in closed form because the gain G varies nonlinearly. Thus a simple iterative method is used to converge to a valid solution.

An important aspect to this solution procedure is to realize that the nonlinear PWM gain G is physically located in the stationary reference frame and is a function of the magnitude of its compensated input error signal. When transformed to the synchronous reference frame, G becomes a function of the magnitude of the error vector as defined in (2):

$$\xi = \sqrt{\xi_q^2 + \xi_d^2}. \quad (2)$$

B. Experimental Verification

The steady-state solutions of the transition mode result in operating points with reduced gain that are a function of both stator current and operating frequency commands. To experimentally verify the proposed model, theoretical solutions are calculated and measured experimentally at various operating frequencies, and the resulting steady-state PWM gain "G" is plotted. The quantity that is plotted is a gain that is normalized to the PWM gain in the linear region of operation. The induction motor is unloaded and operating with constant current commands that produce rated flux. For the theoretical results to correlate with the experimental results it was necessary to incorporate saturation of the magnetizing inductance into the induction motor model.

The results for the stationary (classical) regulator are shown in Fig. 6. Experimental data points are shown with asterisks and theoretical results predicted by the model are represented with a solid line. This figure shows that the transition region is entered at approximately 50 Hz and at approximately 60 Hz the PWM gain G jumps to 0. This jump corresponds to a discrete jump into six-step voltage operation with a total loss of current and a subsequent gain of 0. The model predicts the reduction in gain well and the premature discrete jump into the six-step region very well.

The deterioration of the stationary regulator's current-regulating ability in the transition region is illustrated in Fig. 7. This figure shows an oscilloscope trace of a commanded phase current and the resulting current in the transition region. They result from a d-axis current command that produces rated flux and a frequency command that results in rated speed. The resulting current is not only out of phase with the current command but also has a different magnitude. The current regulator has completely lost control of the current.

The stationary regulator's discrete jump into six-step voltage operation is just one example of the regulator's undesirable performance in the transition region. The reduction of the PWM gain results in a significantly decreased ability of the stationary regulator to regulate current over the entire transition region. To improve current regulator operation in this region, use of the synchronous regulator, as described in [5], is proposed. Its characteristics in the transition region will now be examined with the aid of the developed model. The proposed PWM inverter model of the transition region is applicable to this current regulator as well as the stationary current regulator.

The results for the synchronous regulator are shown in Fig. 8. This figure shows that the transition region is entered at

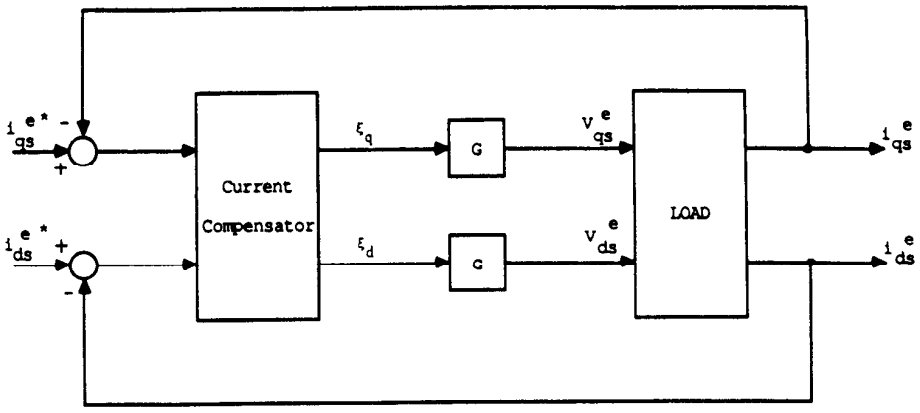

Fig. 5. Current regulator control system model.

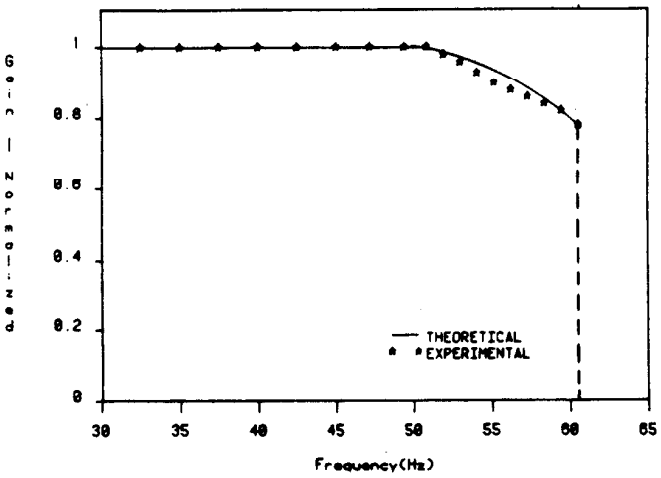

Fig. 6. PWM gain of stationary regulator in transition region.

approximately 50 Hz and extends to approximately 65 Hz, where the PWM gain G smoothly approaches zero. This corresponds to a smooth transition into the voltage six-step region.

Throughout the transition region the synchronous regulator is able to maintain ideal current regulation. This is illustrated in Fig. 9, with an oscilloscope trace of a resulting phase current and command similar to that of Fig. 7. The phase current command is of the same magnitude and frequency as the command in Fig. 7. Despite the fact that the actual current is very nearly a six-step current, its fundamental component has the same magnitide and phase as the command current.

Fig. 10 presents a further illustration of the synchronous regulator's ability to maintain ideal steady-state current regulation over the entire transition region. This figure shows steady-state current-regulation transfer functions in this reduced gain region for the synchronous regulator. Two transfer functions are plotted: i^e_{qs}/i^{e*}_{qs} and i^e_{ds}/i^{e*}_{ds}. The procedure for calculating and measuring these transfer functions will now be outlined. Reference should be made to the system model shown in Fig. 5. The currents in the figure are in the synchronous reference frame, thus in the steady state they are dc at all operating frequencies.

The first step is accomplished by commanding a dc current (i^{e*}_{qs}) into the q-axis while setting the d-axis current command (i^{e*}_{ds}) to zero. The resulting dc currents (i^e_{qs} and i^e_{ds}) are then measured. This procedure is then repeated over an operating frequency range of 0–65 Hz. At each frequency the ratio of output to input current is calculated as the transfer function. Fig. 10 shows there is no deterioration in current regulation as a function of operating frequency. The quantity of q-axis current that results is exactly that which is commanded, while no d-axis current results.

Most of the modeling errors occur as the result of theoretical errors in the describing function technique when used in a closed-loop system. The describing function technique, in its simplest form, assumes that the input into the nonlinear element is always sinusoidal. This is proper for an open-loop system, but when the nonlinear element occurs in a closed-loop system its input is affected by the output of the nonlinear element and is no longer purely sinusoidal.

C. Operation of the Stationary and Synchronous Regulators

In this section the steady-state models developed for the transition region will be used to further illustrate the advantages of the synchronous regulator over the stationary regulator. The model will also be used to gain an insight into the unique characteristics of each regulator in this region.

Fig. 11 shows a steady-state current regulation transfer function of both regulators for an induction motor operating at no load with rated flux. These curves are similar to those of Fig. 10, except that they are for both regulators and show only the i^e_{qs}/i^{e*}_{qs} transfer function. The dashed curve with an asterisk is the current regulation characteristic for the stationary regulator if the current command was reduced so that the inverter remained in the linear region of operation. The other dashed curve is the stationary regulator when the current command is high enough to force transition region operation. The point of deviation of the two stationary regulator curves denotes the start of the transition region. The stationary regulator curves stop abruptly because of the jump into six-step operation, while the synchronous regulator continues to regulate without error to almost 65 Hz in the transition region.

As illustrated in Fig. 11, the synchronous regulator can regulate current without error over a wide range of frequen-

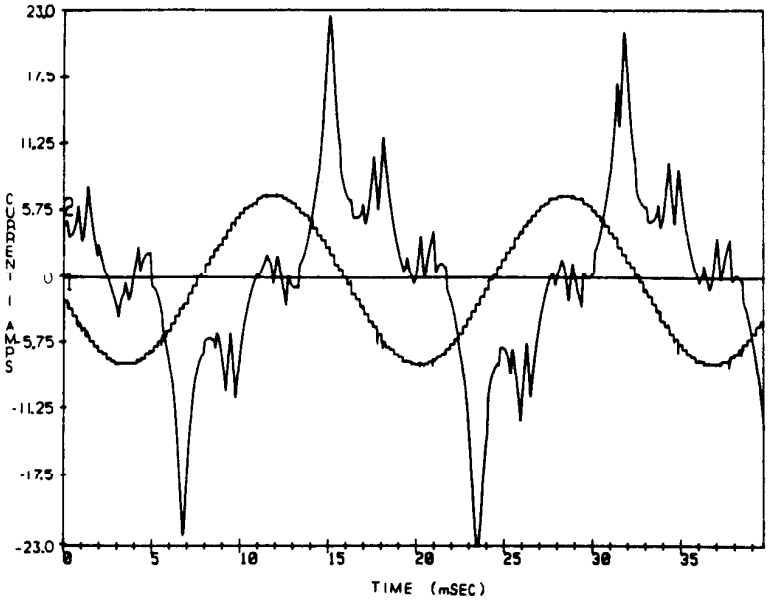

Fig. 7. Oscilloscope trace of phase current command and resulting current in transition region for stationary regulator.

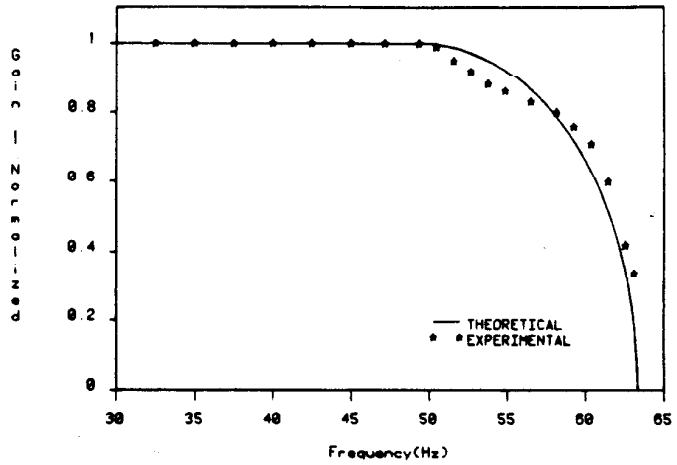

Fig. 8. PWM gain of synchronous regulator in transition region.

cies. This steady-state regulation can be achieved as long as the bus voltage is of sufficient magnitude to produce a fundamental component magnitude of voltage that can drive the commanded current through the motor impedance. This regulation occurs despite the fact that the effective proportional and integral gains of the regulator are decreasing due to pulse-dropping. This is a result of an inherent characteristic of the synchronous regulator that was demonstrated in [5]. There it was shown that the steady-state performance of the synchronous regulator is independent of compensator gains.

To directly compare the performance of the synchronous regulator with the stationary regulator, the gain G is plotted as a function of operating frequency for both regulators in Fig. 12. These plots are generated using the developed model and assume constant magnetizing inductance for the induction motor. This figure clearly shows that the characteristics of the synchronous regulator enable it to fully utilize the bus capabilities of the drive, despite the pulse-dropping phenomenon. This example demonstrates that through the use of the synchronous regulator rather than the stationary regulator, the speed range over which the current can be controlled can be extended by 25 percent at a rated flux condition. A similar example could be shown in which the flux range over which the current can be controlled can be extended by 25 percent at a rated speed condition.

To illustrate the additional capabilities of the synchronous regulator at speeds higher than base speed, capability curves will be generated. Fig. 13 shows the maximum flux-producing (no load) current that can be controlled as a function of frequency for both regulators. Controllable current means that the regulator has not entered the six-step region of operation: for the stationary regulator it does not imply that there are no errors in the current regulation.

The problem of the stationary regulator's discrete jump into

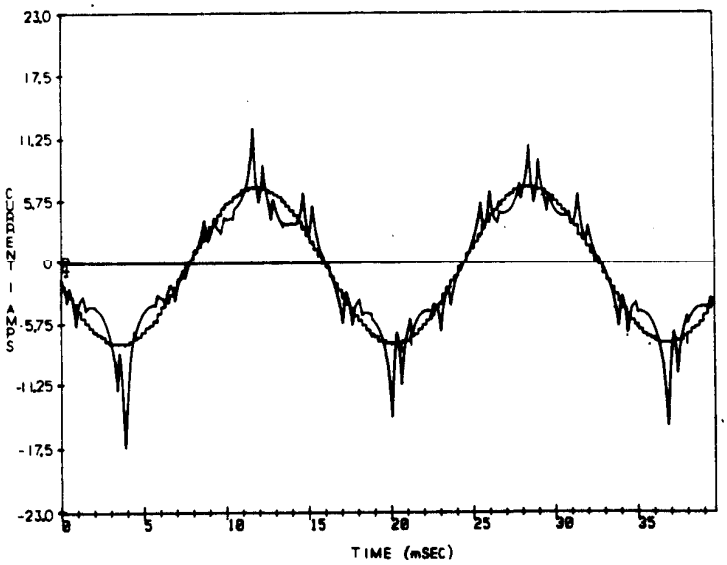

Fig. 9. Oscilloscope trace of phase current command and resulting current in transition region for synchronous regulator.

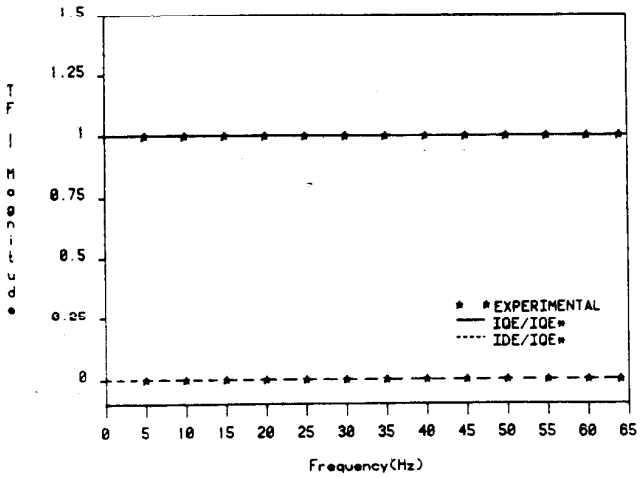

Fig. 10. Steady-state current regulator transfer functions of synchronous regulator.

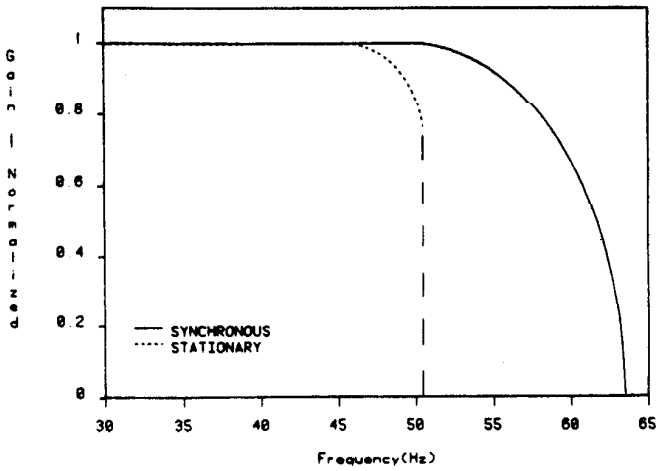

Fig. 12. PWM gain of stationary and synchronous regulators.

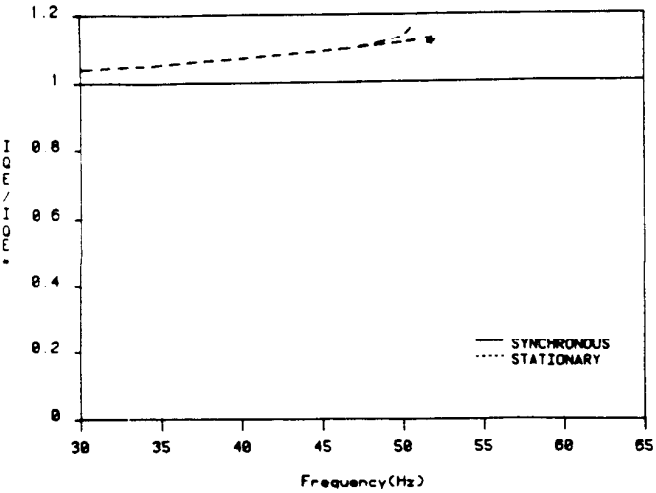

Fig. 11. Steady-state current regulator transfer functions of stationary and synchronous regulators.

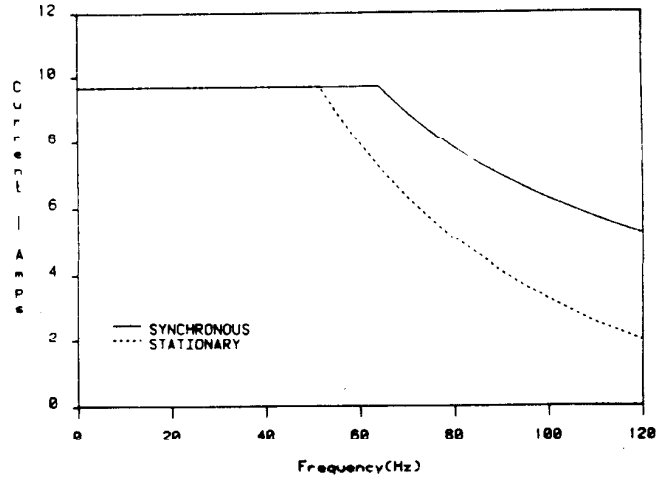

Fig. 13. Capability curves of stationary and synchronous regulators in transition region.

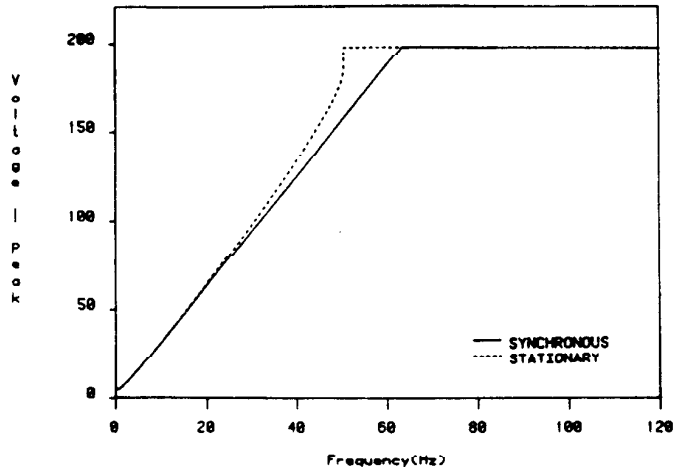

Fig. 14. Induction motor terminal voltage of stationary and synchronous regulators.

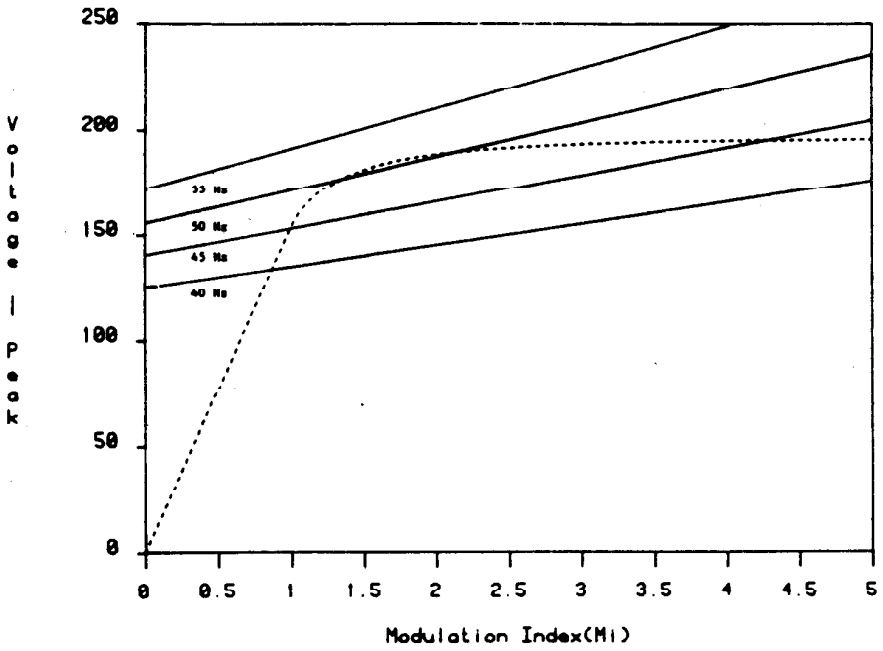

Fig. 15. Load lines at various operating frequencies for stationary regulator.

the six-step region is illustrated in Fig. 14. This figure shows the magnitude of the motor voltage for both regulators in both the linear and transition region. The stationary regulator voltage snaps into six-step at about 50 Hz and at about only 90 percent of the inverter's full voltage. Conversely, the synchronous regulator moves smoothly into six-step operation.

Some insight into this problem can be gained from the iterative solution method of the model. Fig. 15 shows the input–output relationship of the PWM inverter from Fig. 3 as a dashed curve. Also shown are "load lines" at various operating frequencies for a stationary current-regulated motor at no load and rated flux. Each line is generated by calculating a locus of linear steady-state solutions as a function of PWM gains "G." The points where the line intersects the dashed curve represent the potential operating points for that frequency. As operating frequency is increased the intersection points occur at higher and higher voltages on the dashed curve. This continues until suddenly there is no intersection point, and hence there is no valid steady-state solution. This corresponds to the inverter's discrete jump into six-step operation and occurs at a voltage lower than the maximum output. It should be noted that for each load line there are two potential operating points. The operating point at the lower modulation index corresponds to the operating point in the experimental results. The operating point that occurs at the higher modulation index can be shown to be dynamically unstable.

Fig. 16 shows similar curves for the synchronous regulator. For this regulator the load lines have zero slope and always

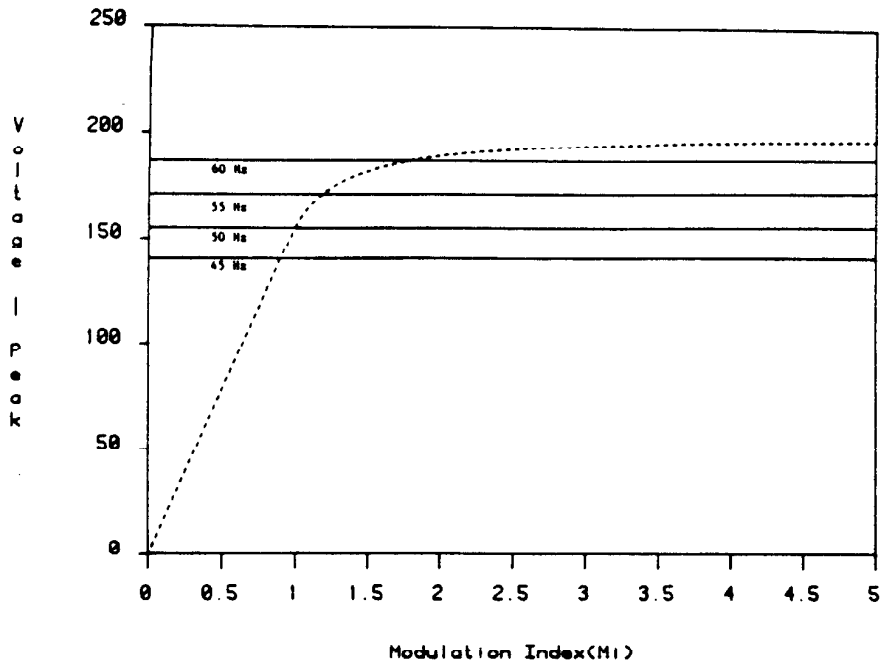

Fig. 16. Load lines at various operating frequencies for synchronous regulator.

provide an intersection with the dashed curve until the maximum inverter voltage is reached.

III. Transient Operation

This section presents analytical and test results of the transient operation of the current regulators in the transition region. The analysis will require a system model in which the nonlinear gain G is linearized about a steady operating point. This model will then be experimentally verified.

A. Linearization Procedure

The fundamental component model of the nonlinear PWM gain element is shown in Fig. 3 as an input–output relationship. The chord slope of this relationship represents the steady-state gain and is used in the steady-state solution. This gain, however, is not appropriate for the small-signal model because the small-signal transients respond to the tangent slope of a particular operating point on the curve. Thus it is necessary to linearize the system around a valid steady-state operating point.

The linearization procedure requires a formulation of the system equations where the nonlinear gain "$G(\xi)$" appears explicitly. It is then necessary to take the partial derivatives of each equation with respect to each state variable and input of which G is a function. These partial derivatives are then evaluated at the operating point and used to modify the system equations. Reference [12] presents in detail the development of the small-signal model for the synchronous regulator when operating in the transition region.

B. Experimental Verification

To verify the proposed small-signal model, frequency response measurements of the i^e_{qs}/i^{e*}_{qs} transfer function will be measured at rated operating frequency. The results, shown in Fig. 17, are presented in the form of Bode plots. The plots are generated in a manner similar to that which generated the steady-state results of Figs. 10 and 11. Those steady-state results were generated by commanding a dc current (synchronous) in the q-axis and measuring the resulting dc current (synchronous) in the d and q axes. The procedure was performed over an operating frequency range of 0–65 Hz. The frequency response plots are generated by again commanding a dc current in the q-axis, except with a small-signal frequency superimposed on the dc command. This frequency command is varied from 0 to 1500 Hz, and the magnitude and phase of the corresponding frequency is measured on the q-axis output. The tests were performed in an induction motor at no load and at rated operating frequency. A summary of the results is presented in this paper.

Fig. 17 shows the magnitude and phase plots of the i^e_{qs}/i^{e*}_{qs} transfer function. This figure shows a bandwidth of 350 Hz, which is significantly reduced from the linear region bandwidth of 750 Hz. The data verifies the bandwidth calculation well and also predicts a small resonance at a frequency of 5 Hz. These characteristics cannot be predicted by an appropriate simple reduction in the chord slope of the PWM gain G in the linear model. Thus the linearization procedure was necessary to predict the small signal response of the current regulator in the transition region.

The experimental correlation with the peak values of the magnitude portion of the Bode plot in Fig. 17 is not very good. This is partially due to the fact that good frequency response measurements are very difficult to obtain in the region. Due to the large number of pulses being dropped by the inverter, the resulting currents closely resemble six-step

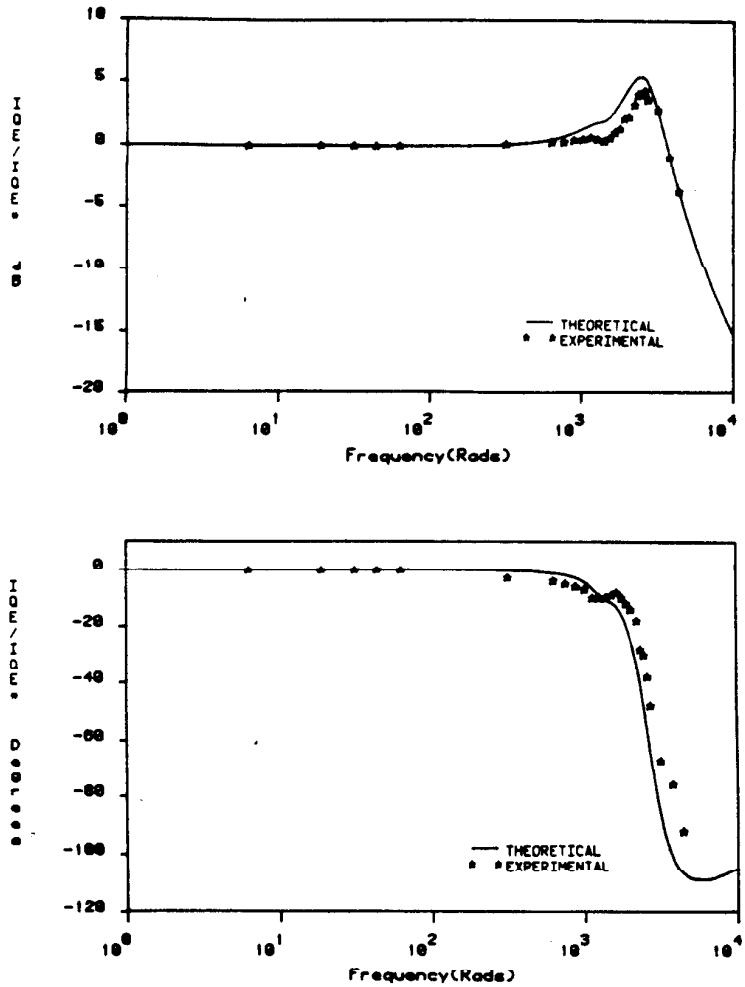

Fig. 17. Synchronous regulator self-coupling current transfer function. $i_{ds}^{e*} = 0$; $i_{qs}^{e*} = 9.66$ A.

currents and thus have higher harmonics which distort the frequency response measurements.

C. Operating Characteristics

Fig. 17 demonstrated a reduction in bandwidth for the current regulator in the transition region due to the loss of PWM gain. This bandwidth reduction is due to the migration of the poles associated with the stator of the induction machine to a region of less damping. Fig. 18 shows a root locus of the dominant stator poles of the synchronous regulator/motor as it smoothly transitions from current-regulated operation to voltage-source operation. The lightly damped stator poles corresponding to voltage source operation have deteriorated to the value of the stator transient time constant of the motor itself.

IV. Conclusion

The authors have presented a model for naturally sampled CRPWM inverters operated in the transition region. This model was used to explain the significant differences between the classical (stationary) and synchronous regulator's performance in this region. Among the differences is the precipitous reduction in gain associated with the stationary regulator while the synchronous regulator exhibits a controlled reduction in gain as operating frequency or commanded current increases; the stationary regulator's inability to accurately regulate current at or above the frequency rating of the drive while the synchronous regulator is capable of steady-state current regulation without error over the entire frequency range of operation; the stationary regulator's discontinuous voltage characteristic as six-step operation approaches while the synchronous regulator is linear. Finally, the model accurately predicted the synchronous regulator's reduction in bandwidth and its continuous migration into six-step voltage inverter operation.

Appendix

Induction Motor Data

5.0 hp	NEMA Design B
$r_s = 0.56\ \Omega$	$L_{ls} = L_{lr} = 0.0036$ H
$L_m = 0.074$ H	$r_r = 0.22\ \Omega$
$J = 0.0158\ \text{kg}-\text{m}^2$	

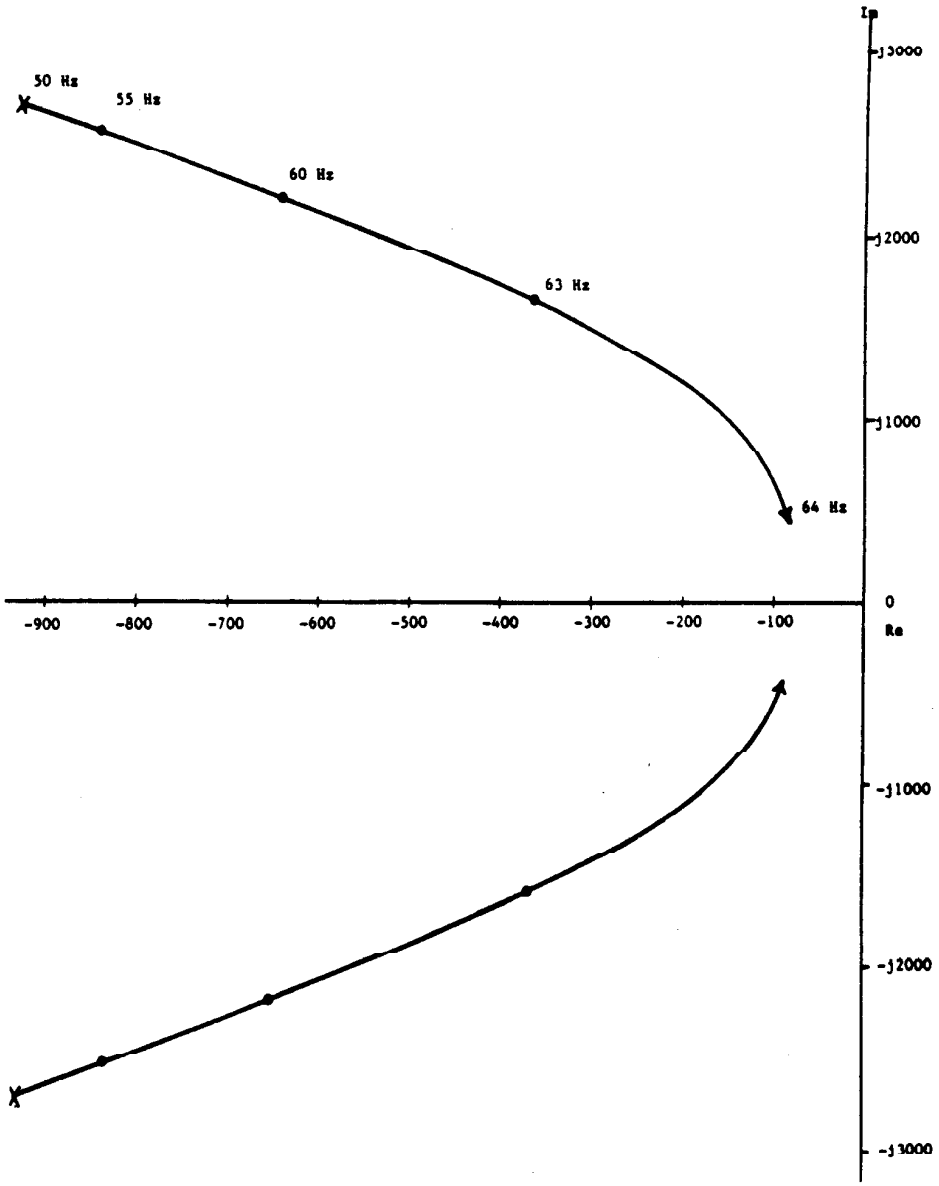

Fig. 18. Dominant stator poles of synchronous regulator in transition region.

ACKNOWLEDGMENT

The authors wish to acknowledge the technical assistance of Mr. D. Leggate during this research.

REFERENCES

[1] D. M. Brod and D. W. Novotny, "Current control of VSI-PWM inverters," in *Conf. Record of IEEE-IAS Annual Meeting*, Sept. 30-Oct. 4, 1982; pp. 418-425.

[2] H. Nagase, Y. Matsuda, K. Ohnishi, H. Ninomiya, and T. Koike, "High performance induction motor drives," in *Conf. Record of IEEE-IAS Annual Meeting*, Oct. 3-7, 1983; pp. 596-603.

[3] S. Meshkat and E. K. Persson. "Optimum current vector control of a brushless servo amplifier using microprocessors," in *Conf. Record of IEEE-IAS Annual Meeting*, Sept. 30-Oct. 4, 1984; pp. 451-457.

[4] H. Ikejima, M. Nomura, H. Sugimoto, and E. Ohno, "Microprocessor-based ac motor drive control for elevator," in *Conf. Record of 1983 IEEE Power Electronics Specialists*, pp. 64-69.

[5] T. M. Rowan and R. J. Kerkman, "A new synchronous current regulator and an analysis of current regulated PWM inverters," in *Conf. Record of 1985 IEEE-IAS Annual Meeting*, pp. 487-495.

[6] G. B. Kliman and A. B. Plunkett, "Development of a modulation strategy for a PWM inverter drive," *IEEE Trans. Ind. Appl.*, vol. IA-15, no. 1, pp. 72-79, Jan./Feb. 1979.

[7] P. D. Ziogas, "The delta modulation technique in static PWM inverters," *IEEE Trans. Ind. Appl.*, vol. IA-17, no. 2, pp. 199-204, Mar./Apr. 1981.

[8] T. Ohnishi and H. Okitsu, "A novel technique for three phase inverter/converter," in *Conf. Record of 1983 IPEC*, Tokyo, Japan, pp. 384-395.

[9] P. C. Sen and G. Premchandran, "Improved PWM control for inverters and induction motor drives," *IEEE Trans. Ind. Electron.*, vol. IE-31, no. 1, pp. 43-50, Feb. 1984.

[10] T. H. Chin, M. Nakano, and Y. Fuwa, "New PWM technique using a triangular carrier wave of saturable amplitude," *IEEE Trans. Ind. Appl.*, vol. IA-20, no. 3, pp. 643-650, May/June 1984.

[11] M. Varnovitsky, "Development and comparative analysis of pulse-width modulation strategy," *IEEE Trans. Ind. Electron.*, vol. IE-31, no. 3, pp. 272-276, Aug. 1981.

[12] T. M. Rowan, "Analysis of naturally sampled current regulated pulse-width modulated inverters," Ph.D. thesis, University of Wisconsin—Madison, 1985.
[13] D. Graham and D. McRuer, *Analysis of Nonlinear Control Systems.* New York: John Wiley & Sons, 1961, pp. 77-92.

Timothy M. Rowan (M'87) was born in Milwaukee, WI, in 1958. He received the B.S.E.E. degree with honors from Marquette University, Milwaukee, WI, in 1980, and the M.S.E.E. and Ph.D. degrees from the University of Wisconsin—Madison, in 1982 and 1985, respectively.

From 1979 to 1980 he participated in the cooperative education program at RTE Corporation, Waukesha, WI. He has been employed at the Allen-Bradley Company, Milwaukee, WI, since 1983, where he is currently a Project Development Engineer. His current interests are in the development and analysis of industrial motor drives and starters.

He is a member of Eta Kappa Nu and Tau Beta Pi.

Russel J. Kerkman (S'67-M'76) received the B.S.E.E., M.S.E.E., and Ph.D. degrees in electrical engineering in 1971, 1973, and 1976, respectively, all from Purdue University, Lafayette, IN.

From 1976 to 1980 he was an Electrical Engineer in the Power Electronics Laboratory of Corporate Research and Development of the General Electric Company, Schenectady, NY. While at General Electric, he developed analytical techniques for permanent-magnet motors and contributed to the design and simulation of load commutated converters and synchronous machines as applied to pumped storage hydroelectric applications. He is currently a Principal Engineer at the Allen-Bradley Company. Since joining Allen-Bradley in 1980, he has directed and contributed to the modeling, simulation, and control of custom LSI-based ac drives, and the development of ac current regulators and test procedures for ac motor drives.

Dr. Kerkman was one of 17 Rockwell engineers to receive in 1986 the prestigious Rockwell Engineer of the Year Award.

Thomas A. Lipo (M'64-SM'71-F'87) received the B.E.E. and M.S.E.E. degrees from Marquette University, Milwaukee, WI, in 1962 and 1964, respectively, and the Ph.D. degree in electrical engineering from the University of Wisconsin in 1968. He was an NRC Postdoctoral Fellow at the University of Manchester Institute of Science and Technology, Manchester, England, during 1968-1969.

From 1969 to 1979 he was an Electrical Engineer in the Power Electronics Laboratory of Corporate Research and Development of the General Electric Company, Schenectady, NY. While at General Electric he helped pioneer the computer simulation of many types of converter systems including cycloconverters, pulsewidth-modulation voltage inverters, current-source ASCI inverters, third-harmonic commutated CSI inverters, and load-commutated converters. He also has been heavily engaged in the development of algorithms for solid-state converter drives. He is presently a professor in the Department of Electrical and Computer Engineering, University of Wisconsin—Madison.

Dr. Lipo holds seven patents; another is pending. He has published over 70 technical papers, contributing to the analysis and design of a wide range of industrial applications, including ac drives for ball mills, pumped hydro, and excavators, as well as traction drives for transit cars, locomotives, and off-highway vehicles. He has received seven IEEE Prize Paper Awards, including co-recipient of the 1984 Best Paper Award for the IAS TRANSACTIONS. In 1986 he received the IAS Outstanding Achievement Award for his work in ac motor drives. He is Chairman of the IAS Industrial Drives Committee and serves on the IAS Fractional and Integral Horsepower Subcommittee, the IES Drives Committee, and on the PES Synchronous Machine Subcommittee, the latter of which he is a Past Chairman. He is an Associate Editor of the journal *Electric Machines and Power Systems,* and is Editor of the IEEE TRANSACTIONS ON POWER ELECTRONICS. He is a member of Pi Mu Epsilon, Eta Kappa Nu, Tau Beta Pi, and Sigma Xi.